A Kinetic Model for the Adsorption of Gold from I_2/I^- Solutions onto a Porous Polymer Membrane

M. Pérez-Tello,[1] F. Rodríguez-Felix,[2] M. M. Castillo-Ortega,[2] V. M. Sánchez-Corrales[1]

[1]Departamento de Ingeniería Química y Metalurgia, Universidad de Sonora, Hermosillo, Sonora, Mexico 83000
[2]Departmento de Investigación en Polímeros y Materiales Universidad de Sonora, Hermosillo, Sonora, Mexico 83000

ABSTRACT: A model for the adsorption of gold from I_2/I^- aqueous solutions onto a cellulose acetate (CA)-polyaniline (PANI) porous membrane is presented. The adsorption of gold is represented by an ion-exchange overall reaction in which AuI_2^- ions replace the Cl^- ions at the active sites of the polyaniline matrix. The model incorporates the external mass transfer of AuI_2^- from the bulk solution to the membrane surface, followed by the pore diffusion of AuI_2^- to reach the active sites in the membrane. The overall ion-exchange reaction was assumed to achieve local instantaneous equilibrium. Verification of the kinetic model with the experimental data showed that the effective diffusivity of AuI_2^- within the membrane is about 8.3×10^{-6} cm²/s. The potential applications of the present formulation are discussed. © 2011 Wiley Periodicals, Inc. J Appl Polym Sci 124: 1695–1706, 2012

Key words: diffusion; adsorption; modeling; membranes

INTRODUCTION

The synthesis of polyaniline-based (PANI) composite membranes has received great attention in recent years by the research community. This is because PANI presents a number of characteristics which makes it an excellent candidate for electronic, environmental, and engineering applications. Such properties include good electrical conductivity, chemical stability under environmental conditions, and a suitable ion-exchange capacity.[1–6] Despite its potential, PANI usually is not used as the sole component in membranes. This is because the mechanical strength of PANI is not sufficient to guarantee a long-term use of the material for most applications in which PANI has been tested. Therefore, other materials such as cellulose acetate (CA)[7–9] and poly(methyl methacrylate)[10–12] (PMMA) are mixed with PANI in various proportions to obtain composite membranes with improved mechanical characteristics. The addition of CA and PMMA to PANI typically produces a porous membrane structure which may be particularly useful for potential applications such as adsorption and ion exchange, in which a large surface area for the solid-fluid contact is desirable.

In a previous work,[13] the present authors reported on the synthesis of CA membranes modified with polyacrylic acid using various plasticizers and coated with PANI. The membranes were characterized in terms of their morphology, pore size, electrical conductivity, strain at break, and glass transition temperature. Preliminary experiments showed that one of the formulations of the composite membranes coated with PANI was capable of adsorbing gold from a synthetic gold-iodide (AuI_2^-) aqueous solution at room temperature. This indicated that such a formulation may have the potential to treat aqueous streams typically produced during leaching of gold from ore minerals.[14]

In a subsequent paper,[15] the authors showed that the adsorption equilibrium of gold on the membrane at room temperature followed a Langmuir-type relationship:

$$q_{\text{Aeq}} = \frac{k_1 C_{\text{Aeq}}}{1 + k_2 C_{\text{Aeq}}} \tag{1}$$

where C_{Aeq} and q_{Aeq} are the equilibrium concentrations of gold in the aqueous solution and the solid phase, respectively, and the k symbols are empirically determined parameters. Ion-chromatography analyses of the bulk solution before and after the solid–liquid contact showed that the concentration of total Cl^- ions increased upon the adsorption of gold on the membrane. Early equilibrium stability diagrams[16–18] indicate that under the conditions tested in the experiments, AuI_2^- is the predominant species of gold in the aqueous phase. Therefore, the authors suggested an ion-exchange mechanism by which the AuI_2^- ions adsorbs on the active sites of the PANI structure while the Cl^- ions attached to the PANI structure are simultaneously released to

Correspondence to: M. Pérez-Tello (mperezt@iq.uson.mx).

the aqueous phase. Kinetic experiments conducted in a batch laboratory reactor showed that the bulk concentration of gold did not significantly change after 200 min of operation when the solid/liquid ratio was set to 10 and the initial aqueous concentration of gold was 10 mg/L. The amount of gold adsorbed on the membrane at equilibrium represented about 55% of the gold initially present in the bulk solution.

Previous studies[13,15] showed the potential of the CA-PANI membranes as ion exchangers as well as the main features of this system from an experimental perspective. The goal of this investigation was to develop a mathematical formulation capable of representing the relevant phenomena occurring during the adsorption of gold on the CA-PANI membranes previously studied.

In a recent review of several adsorption mathematical models,[19] Qiu et al. identified two main categories; namely, adsorption reaction models and adsorption diffusion models. Examples of adsorption reaction models include the pseudo-first and pseudo-second order models and the Elovich's equation. These models have been extensively used to fit adsorption kinetic data of a variety of systems.[20–24] Although such formulations may be used for practical applications, they do not provide information concerning the actual phenomena involved during the adsorption process. At the expense of a higher mathematical complexity, a fundamentally based representation of the system may be obtained by means of adsorption diffusion models which incorporate both the reaction kinetics and mass transfer mechanisms within a particular system. Examples of such models are available in the recent literature.[25–29] In this article, an adsorption diffusion model which incorporates external mass transport, pore diffusion, and the nonlinear nature of the adsorption equilibrium isotherm is developed. For that purpose, additional experiments were conducted, as described below.

EXPERIMENTAL

The goal of the experimental program was to provide the relevant data which are necessary to test the model formulation. This includes the membrane apparent density ρ and porosity ε, the Langmuir equilibrium parameters k_1 and k_2, and the kinetics of the gold concentration in the bulk solution, $C_{Ab}^{exp}(t)$. Details of the procedure followed for the synthesis of the membranes are discussed elsewhere[13] and thus are not presented here. CA membranes coated with PANI were used in all the experiments. The membranes were cut into square flat slabs, 1 cm long (L) and 1.27 mm thick (2δ). The length was measured with a Vernier, whereas the thickness was measured by image analysis of scanning electron mi-
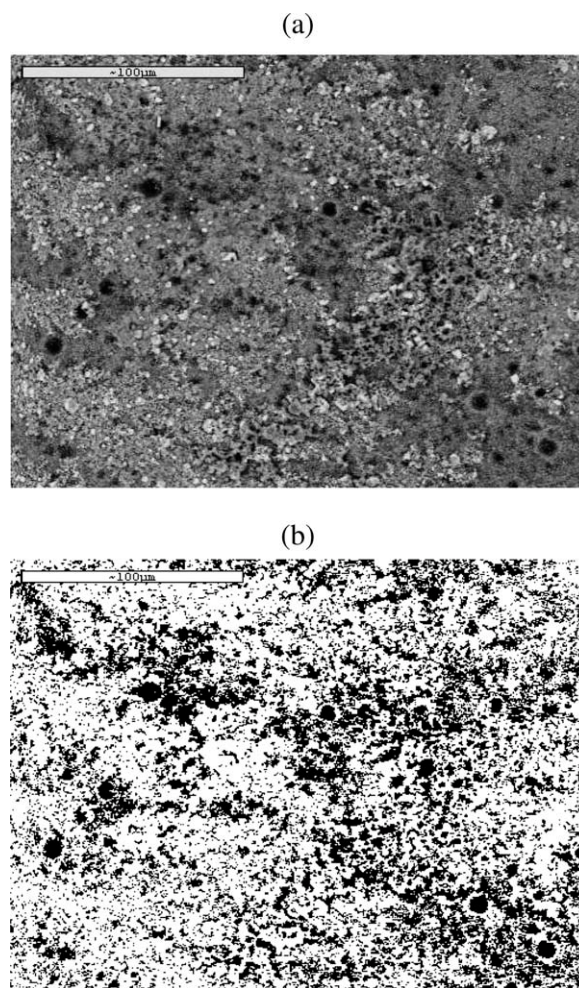

Figure 1 Image analysis of an SEM micrograph of the front side of the CA-PANI membrane; (a) original grayscale image; (b) black-and-white image. The fraction of the area covered by the black spots in (b) was estimated as the membrane porosity.

croscopy (SEM) micrographs of a number of membrane slabs. Both values represent an average over a number of measurements. The apparent density ρ was determined by weighing a specified number n of flat slabs in a scale and dividing the resulting weight w by the total membrane volume, i.e., $\rho = w/(n2L^2\delta)$. The average value obtained from this procedure was $\rho = 164$ g/L.

Current analytical methods do not permit a direct measurement of the membrane porosity ε. Palacio et al.[30] pointed out the experimental difficulties associated in the measurement of this property and discussed the reproducibility of different techniques. In this work, an estimation of the membrane porosity was obtained from digitized SEM micrographs of the membrane surface, as shown in Figure 1. The original SEM images [Fig. 1(a)] were transformed into black and white images [Fig. 1(b)] by means of the Image Tool (IT) software.[31] The fraction of black
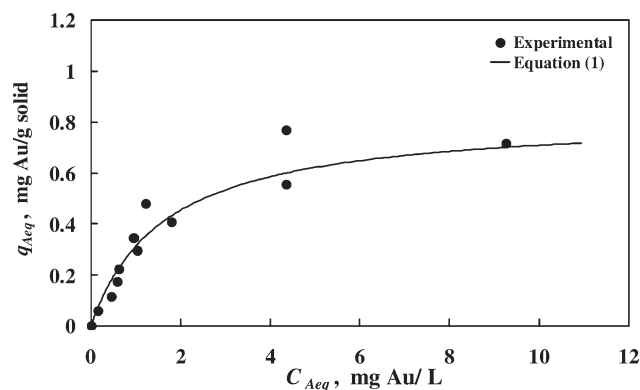
Figure 2 Equilibrium conditions for the adsorption of gold on PANI membranes at 25°C.

area in the latter images computed by the IT software was considered to be the membrane porosity.

The above procedure is based on the assumption that all the pores in the membrane are mostly straight and their length is the same as the membrane thickness. Whereas the SEM images[13] clearly showed that this hypothesis does not apply in this case, it is of interest to note that the average porosity estimated from SEM images of the front sides of the membranes, such as Figure 1, was fairly equal to that obtained from SEM images of the membrane thickness (not shown). This suggests that the average void fraction within the membrane is fairly uniform even though the membrane structure is not symmetric. From the above procedure, the average porosity was estimated to be $\varepsilon = 0.34$.

For the adsorption experiments, a prespecified mass of the membrane flat slabs were weighed and placed into a 125-mL Erlenmeyer flask. The initial gold solution was prepared by dissolving 10.46 g of potassium iodide (Fermont, 99.99% purity) and 4 g of elemental iodide crystals (Fermont, 99.99% purity) into a small volume of distilled water. This mixture was transferred into a 1-L volumetric flask, and additional distilled water was added up to complete 1 L of solution. The resulting solution contained 12 g/L of total iodine. A weighed mass of powdered metallic gold was then dissolved into this solution to obtain the prespecified gold concentration for a given experiment. A sample of the initial solution thus prepared was further analyzed by atomic absorption spectroscopy to verify the gold concentration. The solution was transferred into the 125-mL Erlenmeyer flask in which the membrane flat slabs were previously introduced. All the adsorption experiments were conducted at 25°C under a constant stirring speed of 155 rpm provided by a magnetic stirrer.

In the equilibrium experiments, the initial gold concentration was varied in the range of 2.5–20 mg/L. The solid and liquid phases were allowed to con-

tact for 12 h, after which the membrane slabs were taken out of the Erlenmeyer flask. A sample of the remaining solution was analyzed by atomic absorption spectrometry to determine its gold concentration. The corresponding concentration of gold on the membrane was then calculated from a mass balance of gold in the system:

$$q_{\text{Aeq}} = \frac{V(C_{\text{Ab0}} - C_{\text{Aeq}})}{w} \qquad (2)$$

Figure 2 shows the equilibrium data as well as the Langmuir isotherm obtained from eq. (1). A good agreement between the calculated and the experimental values is observed. The corresponding parameters for eq. (1) were found to be $k_1 = 0.505$ L/g and $k_2 = 0.612$ L/mg.

The kinetic experiments were conducted under the conditions shown in Table I with a solution volume $V = 0.1$ L. Two initial gold concentrations in the aqueous phase were tested: 5 and 10 mg/L. The procedure was similar to that followed in the equilibrium experiments. Individual experiments were conducted up to a prespecified contact time, upon which the solids were taken out of the reaction vessel, and the remaining solution was analyzed to determine the bulk gold concentration $C_{\text{Ab}}(t)$ by atomic absorption spectroscopy. This procedure was repeated at longer contact times until the bulk concentration of gold from one experiment to the next did not change substantially. The bulk kinetic data were found to obey the following expression:

$$C_{\text{Ab}}(t) = a + be^{-t/t_1} + ce^{-t/t_2} \qquad (3)$$

where all the symbols are defined in the nomenclature. It is noted that parameters a, b, c, t_1, and t_2 are empirical; thus no physical significance may be attributed to them. Their values are shown in Table I. Equation (3) was used to represent the overall kinetics in the bulk solution, which was further coupled to the kinetic model describing the adsorption of gold within the membrane, as described below.

TABLE I
Experimental Conditions for the Kinetics Experiments and Parameters for eq. (3)

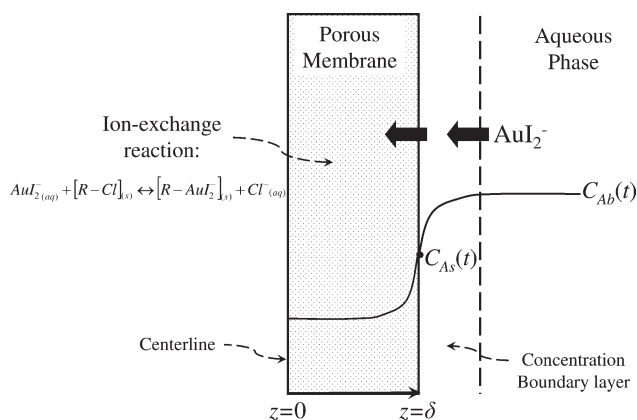|	Symbol	Run 1	Run 2
Initial gold concentration (mg/L)	$C_{\text{Ab}}(0)$	5	10
Number of slabs in the reactor	n	28	48
Parameters for eq. (3):			
mg/L	a	2.3	4.2
mg/L	b	2.0	5.9
mg/L	c	0.61	0
s	t_1	7380	7620
s	t_2	318	0

Figure 3 Schematic representation of the present model.

MODEL FORMULATION

The goal of the present formulation was to represent with reasonable accuracy the adsorption of gold within the membrane observed in the kinetic experiments. Figure 3 shows a schematic representation of the present model. A porous flat membrane with thickness of 2δ is assumed to be in contact with a finite volume V of an aqueous solution containing the initial bulk concentration $C_{Ab}(0)$ of gold. Upon contact, the AuI_2^- ions travel from the bulk solution toward the interior of the porous membrane. Although the reaction mechanism by which gold adsorbs on the active sites is uncertain, it has been proposed[15] that the following ion-exchange reaction represents the overall process:

$$AuI_{2(aq)}^- + [R-Cl]_{(s)} \leftrightarrow [R-AuI_2^-]_{(s)} + Cl_{aq}^- \quad (4)$$
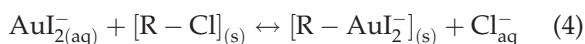
where the subscripts (s) and (aq) refer to the membrane pore surface and the aqueous phase, respectively. The free Cl^- ions thus produced may further react to form other chemical species. Because AuI_2^- is the predominant gold species in solution,[16] its adsorption causes the bulk concentration of gold $C_{Ab}(t)$ in the reactor to gradually decrease in time until overall equilibrium is achieved.

Because the membrane thickness 2δ is much smaller than its length L, the transport of the species was assumed to be unidirectional across the membrane thickness. From the above considerations, a mass balance for the gold within a control volume in the aqueous phase inside the membrane yields

$$\frac{\partial C_A}{\partial t} = D_{Aef} \frac{\partial^2 C_A}{\partial z^2} - \frac{\rho}{\varepsilon}\left(\frac{\partial q_A}{\partial t}\right) \quad (5)$$

Equation (5) states that the rate of accumulation of gold in the liquid phase within the membrane results from two competing phenomena: the rate of diffusion of gold into the control volume as a result of concentration gradients along the pores, and the rate of local adsorption which transfers the gold from the liquid phase to the surface of the pores. Because reaction (4) was assumed to achieve local instantaneous equilibrium, the term in parentheses in eq. (5) may be obtained by differentiation of eq. (1). Further substitution of the resulting expression into eq. (5) yields, upon rearrangement,

$$\frac{\partial C_A}{\partial t} = \alpha(C_A) \frac{\partial^2 C_A}{\partial z^2} \quad (6)$$

where

$$\alpha(C_A) = \frac{D_{Aef}}{1 + \frac{\rho k_1}{\varepsilon(1+k_2 C_A)^2}}. \quad (7)$$

Equation (6) was solved with the following initial and boundary conditions:

$$IC: \quad t = 0, \quad 0 \leq z \leq \delta, \quad C_A = 0 \quad (8)$$

$$BC1: \quad t > 0, \quad z = 0, \quad \frac{\partial C_A}{\partial z} = 0 \quad (9)$$

$$BC2: \quad t > 0, \quad z = \delta,$$
$$-D_{Aef}\frac{\partial C_A}{\partial z} = -k_m(C_{Ab}(t) - C_{As}(t)). \quad (10)$$

The IC establishes that prior to the contact of the membrane with the aqueous solution, no gold is initially present inside the membrane. Because both sides of the membrane are assumed to be exposed to the aqueous phase, BC1 specifies a symmetry condition with respect to the centerline. BC2 is based on the assumption that a concentration boundary layer is formed around the membrane surface, as shown in Figure 3. It expresses the continuity of the flux of gold at the membrane-solution interface, i.e., the rate of transport of gold from the bulk solution to the membrane surface is equal to the rate of diffusion of gold from the surface to the interior of the membrane.

A mass balance for the gold in the bulk solution under unsteady-state conditions yields

$$V\frac{dC_{Ab}(t)}{dt} = -Snk_m(C_{Ab}(t) - C_{As}(t)) \quad (11)$$

in which the solution volume V was assumed to be constant. Equation (11) states that the rate of mass loss of gold from the bulk solution is due to the transport of gold from the bulk to the surface of all the slabs in the reactor. Rearrangement of eq. (11) yields

$$C_{As}(t) = C_{Ab}(t) + \frac{V}{k_m Sn}\frac{dC_{Ab}(t)}{dt} \quad (12)$$

which explicitly relates the instantaneous concentration of gold at the membrane surface $C_{As}(t)$ with

TABLE II
Calculated Values of the Effective Diffusivity and Mass Transfer Coefficient for the Experimental Runs

	D_{Aef} (cm²/s)	k_m (cm/s)	r^2
Run 1, C_{Ab} (0)=5ppm	8.1×10^{-6}	5.95×10^{-1}	0.983
Run 2, C_{Ab} (0)=10ppm	8.5×10^{-6}	1.15×10^{-4}	0.944

that in the bulk solution, $C_{Ab}(t)$. In this expression, k_m represents the system capacity for the transport of gold from the bulk solution to the membrane surface. It is strongly dependent upon the hydrodynamic conditions prevailing in the reactor. In the general case, the value of k_m is relatively small so that eq. (12) yields $C_{As}(t) < C_{Ab}(t)$, which indicates the presence of a concentration boundary layer around the membrane, as shown in Figure 3. In this case, the rate of adsorption of gold is determined by both pore diffusion and external mass transfer effects.

Under perfectly mixed conditions, k_m is a large number, and eq. (12) reduces to $C_{As}(t) = C_{Ab}(t)$. In this case, there is no resistance to interface mass transfer and the concentration boundary layer around the membrane vanishes. Under such conditions, the rate of adsorption is controlled by the diffusion of the gold through the pores of the membrane matrix. A third case arises when the mixing of the solid–liquid suspension is poor, k_m is a small number, and the rate of adsorption is controlled by the interface mass transfer. This latter case may also occur if the membrane is highly porous and the slabs react uniformly throughout its volume. In this case, the rate of adsorption will be limited by the capacity of the bulk solution to transport the gold to the active sites within the slabs.

A complementary expression is obtained by writing a macroscopic mass balance for the gold in the reactor:

$$VC_{Ab}(0) = 2n\varepsilon \int_0^\delta L^2 C_A dz + 2n\rho \int_0^\delta L^2 q_A dz$$
$$+ VC_{Ab}(t) \quad (13)$$

Equation (13) states that the total amount of gold in the reactor at any time is to be distributed into the aqueous phase filling up the pores of the membrane, the surface of the pore walls, and the bulk solution in the reactor. Equation (13) completes the formulation.

The solution of eq. (6) subject to the initial and boundary conditions (8) through (10) and the mass balance restrictions given by eqs. (11) and (13) was done numerically by means of a semi-implicit finite-difference algorithm. Details of the numerical strategy are discussed in the Appendix. In a typical cal-

culation, the values of k_m and D_{Aef} were set, and eq. (6) was solved to yield the aqueous phase concentration profile (C_A versus z). The solid-phase concentration profile (q_A versus z) was computed next from eq. (1). The bulk concentration of gold in the reactor $C_{Ab}(t)$ was then computed by an iterative procedure involving eqs. (10), (11), and (13). This value is to be designated as $C_{Ab}^{cal}(t)$. Upon reaching the final reaction time, the correlation parameter r^2 was computed from the following expression:

$$r^2 = 1 - \frac{\sum\limits_{i=1}^m \left[C_{Ab}^{exp}(t) - C_{Ab}^{cal}(t) \right]^2}{\sum\limits_{i=1}^m \left[C_{Ab}^{exp}(t) - \overline{C_{Ab}^{exp}(t)} \right]^2} \quad (14)$$

where $C_{Ab}^{exp}(t)$ is the experimental value obtained from the empirical expression given by eq. (3), $\overline{C_{Ab}^{exp}(t)}$ is the mean of all the experimental values up to the total time of simulation, and m is the number of experimental data. Symbol r^2 defined by eq. (14) tends to unity as the predicted values approach the experimental values.

For a given experiment, the values of both k_m and D_{Aef} were varied iteratively until the correlation parameter r^2 was as close to unity as possible. For this purpose, the multidimensional Simplex optimization algorithm[32] was used. The optimization of k_m and D_{Aef} values was typically achieved within 400 iterations. For numerical purposes, the mass transfer coefficient k_m was allowed to take on values as large as possible, thus approaching the limiting case of perfect mixing. The lower limit $k_{m, low}$ was established from the physical restriction that $C_{As}(t)$ may not be negative. By setting $C_{As}(t) = 0$, eq. (12) may be rewritten to yield

$$k_{m,low} = -\frac{V}{Sn} \left[\frac{dC_{Ab}(t)/dt}{C_{Ab(t)}} \right] \quad (15)$$

The value of $k_{m,low}$ for which $C_{As}(t)$ remained positive throughout the calculations was typically found when the right-hand side of eq. (15) was computed at $t = 0$.

DISCUSSION OF RESULTS

Table II shows the calculated values for the effective diffusivity D_{Aef} and the mass transfer coefficient k_m for both experiments shown in Table I. Also shown are the values of the correlation parameter r^2 obtained from eq. (14). The D_{Aef} values are fairly constant, with an average of 8.3×10^{-6} cm²/s. This result indicates that the capacity for the AuI_2^- ions to travel through the membrane porous matrix was not substantially affected when the bulk
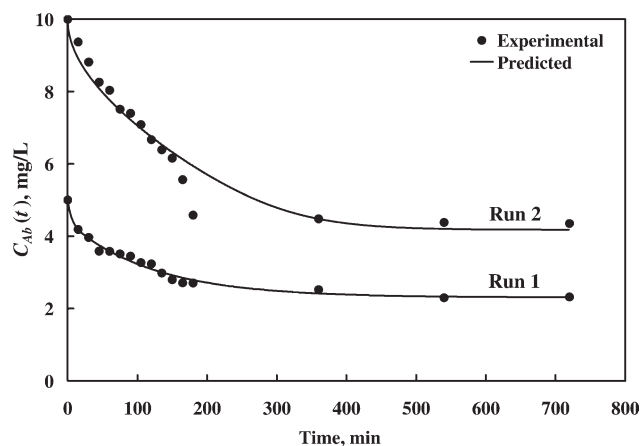
Figure 4 Experimental and predicted values of gold concentration in the bulk solution during the adsorption experiments.

concentration of gold was varied in the range of 5–10 mg/L. This may be explained as follows. The effective diffusivity is defined by[33]:

$$D_{Aef} = D_{Ab}\frac{\varepsilon}{\tau} \tag{16}$$

where D_{Ab} is the molecular diffusivity of the gold complex in the bulk solution, ε is the membrane porosity, and τ is the tortuosity of the diffusion path. For liquids, the molecular diffusivity D_{Ab} is concentration-dependent and tends to the asymptotic value of D_{Ab}^0 as the solute concentration approaches zero.[33] Because the gold solutions used in this study were very dilute, it is expected that $D_{Ab} \cong D_{Ab}^0$, and thus D_{Aef} obtained from eq. (16), be essentially constant. Typical values of D_{Ab}^0 for ionic species in water are of the order of 10^{-5} cm^2/s.[34] This yields D_{Aef} values from eq. (16) of the order of 10^{-6} cm^2/s. The average value of D_{Aef} obtained in this study ($D_{Aef} = 8.3 \times 10^{-6}$ cm^2/s) is in good agreement with the expected order of magnitude.

Table II also shows that k_m for run 1 was three orders of magnitude higher than that obtained for run 2. This suggests that the degree of mixing achieved in run 1 was more efficient than that achieved in run 2. Because all the kinetic experiments were conducted at a constant stirring speed of 155 rpm, at first glance this result seems to be contradictory. A possible explanation for this behavior is based on the fact that the number of membrane slabs used in run 1 (28) was considerably lower than that used in run 2 (48). The higher density of the solid-liquid suspension in run 2 may have affected the hydrodynamic conditions around the slabs and thus decreased the efficiency of the transport of gold from the bulk solution to the membrane surface. This in turn may have affected the thickness of the concentration boundary layer around the slabs.

The above discussion is relevant in the present context because there are practical limitations for the degree of mixing that can be used in this type of a system. If the stirring speed is too low, the hydrodynamic conditions around the slabs may not be uniform and the rate of adsorption within the slab population will be uneven. On the other hand, a very high stirring speed may cause physical damage to the slabs as a result of their contact with the stirrer and the reactor walls. This result suggests that in the analysis of kinetic data in which membrane slabs are suspended in a batch reactor, care must be taken to incorporate mass transfer effects for the appropriate interpretation of experimental data.

Because the rate of adsorption of gold within the CA-PANI membrane was controlled by both interface mass transfer and pore diffusion, improvements in the adsorption rate may be expected if either D_{Aef} or k_m are increased. The increase of k_m may be difficult because of the practical limitations discussed above. On the other hand, according to eq. (16) the effective diffusivity D_{Aef} may be increased by increasing the membrane porosity, decreasing the membrane tortuosity, or both. This provides directions for further developments on the synthesis of CA-PANI membranes with improved characteristics.

Figure 4 shows the experimental and predicted values for the bulk concentration of gold $C_{Ab}(t)$ during the adsorption experiments. The predicted curves were calculated with the numerical values of D_{Aef} and k_m shown in Table II. Good agreement between the predicted and the experimental values is observed in both runs, which supports the hypotheses of the present formulation. The best agreement was obtained for run 1, in which the predicted values closely match the experimental data. For run 2, the model overestimated the bulk concentration within the interval of 150–180 min. Replicated experiments under these conditions showed no significant variations of the experimental data. Therefore, this behavior is likely due to a factor not included in the present formulation and deserves further investigation.

Because the model was capable of predicting with good accuracy both the kinetics and the final equilibrium conditions in the reactor, it may be used to analyze the main features of the experimental system. Figure 5 shows the predicted concentration profiles of gold in both the liquid phase filling up the pores [Fig. 5(a)] and the solid phase [Fig. 5(b)] for run 1. The results obtained for run 2 were similar to those shown in Figure 5 and thus are not shown. Figure 5(a) shows steep concentration gradients in the vicinity of the membrane surface during the first minutes of contact. As expected, the concentration gradients gradually decrease and tend to vanish across the slab thickness as time progresses. The
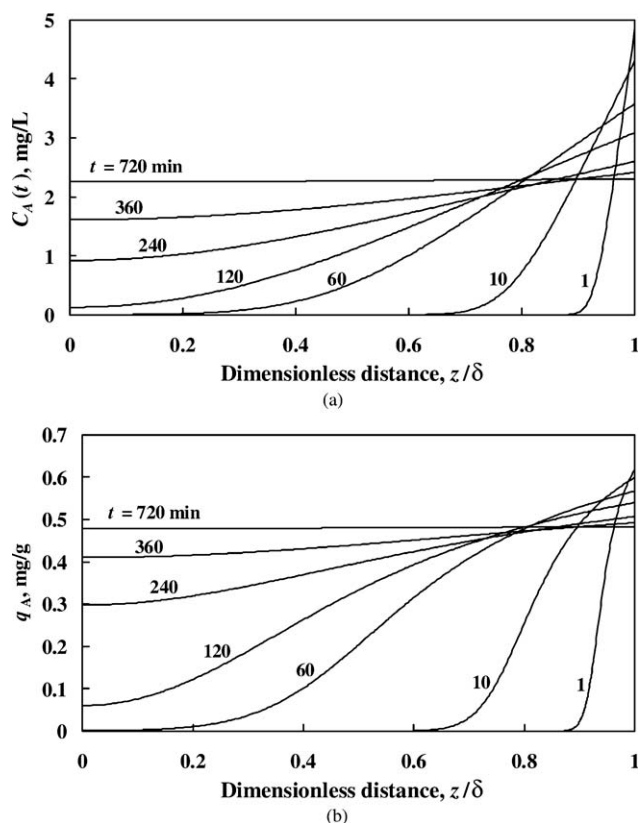
Figure 5 Evolution of the gold concentration profiles within the membrane during adsorption: (a) liquid phase in the pores; (b) solid phase. Initial gold concentration in the bulk solution: 5 mg/L.

gold complex reaches the center of the membrane in approximately 300 min, and it takes additional 420 min to reach overall equilibrium.

Figure 5(b) shows the corresponding prediction for the concentration profiles of gold in the solid phase. In this case, the concentration profiles show a sigmoidal shape as a result of the equilibrium relationship [eq. (1)], which holds locally within the membrane. It is noted that at some locations in the vicinity of the membrane surface ($0.9 < z/\delta < 2$), q_A increases rapidly at early stages of the process and further decreases until overall equilibrium is achieved. This behavior also results from the assumption of local chemical equilibrium [eq. (1)] and indicates that in the vicinity of the membrane surface, some of the gold adsorbed at the early stages of the process is further desorbed in order for the entire slab to achieve equilibrium.

Because the number of active sites in the membrane was estimated to be in large stoichiometric excess to carry out reaction (4), the long reaction time required to achieve equilibrium may be attributed to several factors: first, the relevance of mass transfer and pore diffusion, which hinders the transport of the AuI_2^- ions from the bulk solution to the active sites within the membrane; and second, the

presence of other anions in the aqueous solution, such as I^- ions, which compete for the active sites within the membrane and thus decrease the number of active sites available for the adsorption of the AuI_2^- ions.

Whereas the kinetics of gold adsorption strongly depends on the values of the effective diffusivity D_{Aef} and the mass transfer coefficient k_m, the final equilibrium conditions are completely determined by the initial amounts of the species in the reactor and thermodynamic considerations. Therefore, they may be computed in advance from eq. (13) by setting $t = \infty$. At equilibrium, the gold concentrations in the liquid and solid phases become $C_{A\infty}$ and $q_{A\infty}$, respectively, and are constant throughout the slabs. Therefore, the integrations in the right-hand side of eq. (13) may be done analytically; further substitution of eq. (1) into eq. (13) yields, upon rearrangement,

$$p_1 C_{A\infty}^2 + p_2 C_{A\infty} + p_3 = 0 \tag{17}$$

where

$$p_1 = k_2(\varepsilon + \beta) \tag{18}$$

$$p_2 = \varepsilon + \rho k_1 + \beta(1 - k_2 C_{Ab}(0)) \tag{19}$$

$$p_3 = -\beta C_{Ab}(0) \tag{20}$$

$$\beta = \frac{V}{2nL^2\delta} \tag{21}$$

For a given experiment, $C_{A\infty}$ may be calculated from eq. (17) by using the well-known solution to a quadratic algebraic equation. Equations (17) through (21) show that $C_{A\infty}$ is dependent upon the values of the membrane properties (ε, ρ), the initial concentration of gold in the bulk solution $C_{Ab}(0)$, the adsorption equilibrium constants (k_1, k_2), and the ratio of the volumes of the aqueous to the solid phase β. The solution to eq. (17) based on the values shown in Table I yields $C_{A\infty} = 2.3$ and 4.0 mg/L for runs 1 and 2, respectively. The corresponding values shown in Figure 4 for $t = 720$ min are 2.2 and 4.0 mg/L, respectively. Thus, a good agreement between the predicted and the experimental values at equilibrium conditions is observed.

A practical application of the present formulation is the calculation of the fraction of gold initially present in the solution which has been adsorbed on the membrane up to a given time t. This quantity is referred to in the literature as gold recovery or gold uptake. In this study, it is represented by symbol f_{Au} and defined by

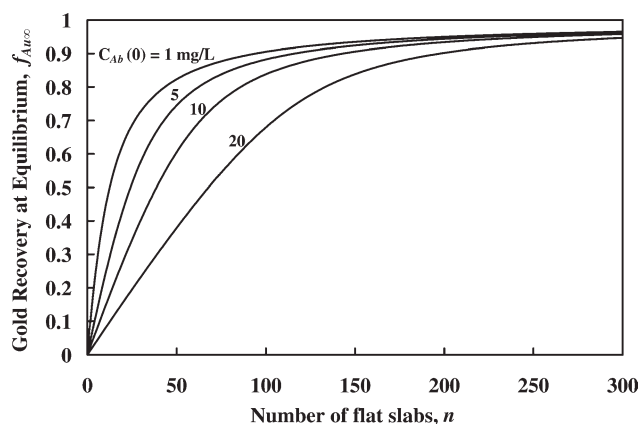$$f_{Au} = \frac{2n\rho \int_0^\delta L^2 q_A dz}{V C_{Ab}(0)} \tag{22}$$

Figure 6 Predicted gold recovery at equilibrium as a function of the initial concentration in the bulk solution and the number of flat slabs in the reactor.

Because the goal of the adsorption process is to transfer the gold from the bulk solution to the active sites within the membrane, it is desirable that f_{Au} becomes as close to unity as possible within a short reaction time. In the present system, the maximum value of f_{Au} is obtained when overall equilibrium is achieved. In this case, eq. (22) becomes

$$f_{Au\infty} = \left(\frac{2\rho L^2 \delta}{V}\right)\frac{n}{C_{Ab}(0)}q_{A\infty} \tag{23}$$

in which the term in parentheses is the mass of a single slab divided by the solution volume. Provided the slabs characteristics—ρ, L and δ and the solution volume V—have been prespecified for a particular system, at first glance, eq. (23) may suggest that $f_{Au\infty}$ is directly proportional to n and inversely proportional to $C_{Ab}(0)$. However, it is noted that $q_{A\infty}$ is not an independent variable but depends upon the values of both n and $C_{Ab}(0)$ through the equilibrium relationships of eqs. (1) and (17). Because both equations are nonlinear in nature, $f_{Au\infty}$ is also a nonlinear function of both n and $C_{Ab}(0)$.

To clarify this point, a series of equilibrium calculations were made in which the number of slabs n and the initial concentration $C_{Ab}(0)$ were varied, and the final gold recovery $f_{Au\infty}$ was computed from eq. (23). During the calculations, the membrane properties: ρ, L and δ, and the solution volume V were set to the experimental values discussed in the previous

section of this article. The results are shown in Figure 6. The values of $C_{Ab}(0)$ and n were varied in the range of 1–20 mg/L and 1–300, respectively. It is noted that all the curves show a linear behavior for relatively small values of n. In this region, the contribution of additional slabs in the reactor has a significant effect on the final gold recovery. The range of the linear region depends on the value of the initial concentration $C_{Ab}(0)$; i.e., the higher the $C_{Ab}(0)$ value, the larger the range and vice versa. Beyond this linear range, further increase in the number of slabs in the reactor contributes less significantly to the final gold recovery, and $f_{Au\infty}$ approaches asymptotically to unity as n tends to infinity.

The behavior of the curves shown in Figure 6 may be explained in terms of Figure 1 and eq. (23), as follows. For a given amount of gold in the bulk solution, the continuous addition of slabs into the reactor provides a larger amount of active sites for the adsorption of gold. If the system is allowed to reach equilibrium, a continuously lower concentration of gold $C_{A\infty}$ will be left in the aqueous phase. According to Figure 1, this in turn causes $q_{A\infty}$ to decrease and asymptotically tend to zero as n tends to infinity. As a result, the product $nq_{A\infty}$ in eq. (23) increases linearly for relatively low values of n and increases more gradually as n tends to infinity. The behavior of this product thus establishes the trends observed. Figure 6 also shows that for a given number of flat slabs in the reactor n the higher $f_{Au\infty}$ is, the lower the $C_{Ab}(0)$ value; i.e., the recovery of gold from dilute solutions is more efficient than recovery from concentrate solutions. Based on the previous discussion regarding the number of active sites provided in each experiment, this was an expected result.

Whereas Figure 6 establishes the maximum gold recovery that may be achieved in the system under particular operating conditions, it provides no information concerning the kinetics of the operation. For this purpose, computer simulation can be used. An example of such a study is shown in Table III. Here, the effects of the initial concentration of gold in the bulk solution $C_{Ab}(0)$, and the number of slabs in the reactor, n on the kinetics of gold recovery are varied for all combinations of the two test variables considered in the experimental study. It is noted that runs 3 and 4 are hypothetical because no experiments

TABLE III
Values of Model Parameters for the Simulation Runs and Final Gold Recovery

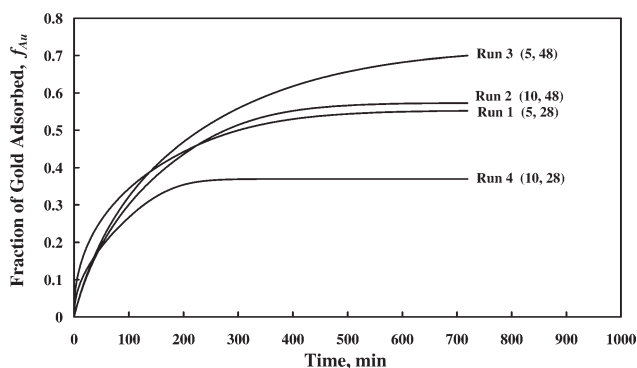| Run no.	$C_{Ab}(0)$ (mg/L)	n	D_{Aef} (cm^2/s)	k_m (cm/s)	$Bi = \frac{k_m\delta}{D_{Aef}}$	$\gamma = \frac{2nL^2\delta\rho}{VC_{Ab}(0)}$	$f_{Au\infty}$
1	5	28	8.3×10^{-6}	5.95×10^{-1}	4552	1.17	0.55
2	10	48	8.3×10^{-6}	1.15×10^{-4}	0.88	1.0	0.57
3	5	48	8.3×10^{-6}	1.15×10^{-4}	0.88	2.0	0.72
4	10	28	8.3×10^{-6}	5.95×10^{-1}	4552	0.58	0.37

Figure 7 Predicted evolution of the fraction of gold adsorbed for runs 1 through 4 in Table III. Numbers in parentheses indicate the initial bulk concentration of gold in mg/L, and the number of flat slabs in the reactor, respectively.

were conducted under such conditions. Thus, no experimental values for k_m and D_{Aef} were available. To overcome these limitations, the following assumptions which are based on the previous discussion of Table II were made. First, the mass transfer coefficient k_m was assumed to be mostly dependent upon the number of flat slabs in the reactor; thus, it was set to the corresponding values shown in Table II; and second, the effective diffusivity D_{Aef} was assumed to be constant and equals to the average value: $D_{Aef} = 8.3 \times 10^{-6}$ cm^2/s. Because the goal of this analysis is to show the potential application of the present formulation and not to provide a rigorous prediction of all cases, the above assumptions are not critical at this stage.

Also shown in Table III are the values of the Biot number, which establishes the relative importance of mass transfer and pore diffusion on the adsorption kinetics. A Biot number close to unity indicates a similar relevance of both phenomena. A Biot number much larger than unity indicates a diffusion-control mechanism, whereas a Biot number much smaller than unity indicates a mass-transfer control mechanism. Table III thus shows two cases of diffusion-control mechanism (runs 1 and 4), and two cases of both diffusion and mass transfer control mechanism (runs 2 and 3). An additional parameter included in Table III is the membrane-to-gold mass ratio, which is defined by

$$\gamma = \frac{2nL^2\delta\rho}{VC_{Ab}(0)} \qquad (24)$$

Symbol γ may be seen as an indirect measurement of the number of active sites provided for the adsorption of gold. Thus, it represents an intensive property with thermodynamic implications on the final recovery $f_{Au\infty}$, as may be inferred from eq. (23), which can be rewritten as $f_{Au\infty} = \gamma q_{A\infty}$.

Figure 7 shows the predicted evolution of f_{Au} for runs 1 through 4. To facilitate the interpretation of results, the values of both $C_{Ab}(0)$ and n are written in parentheses following the designation of each curve. Overall, f_{Au} increases rapidly at short reaction times and becomes asymptotic to the equilibrium value as time progresses. For reaction times less than about 120 min, all curves are close to each other and some of them intersect; thus, no substantial differences in the kinetics of gold recovery are observed. A clear trend is observed after about 300 min, upon which all curves approach the equilibrium values $f_{Au\infty}$. It should be emphasized that the kinetics shown in Figure 7 is determined by the magnitudes of both k_m and D_{Aef}. Thus, it does not represent an intrinsic characteristic of the adsorption reaction. As discussed previously, such a behavior can be modified if changes in the membrane structure and the stirring conditions in the reactor are made.

The main effects of the initial concentration $C_{Ab}(0)$ and the number of slabs in the reactor n on the values of f_{Au} may be observed at long reaction times; i.e., when the system approaches equilibrium. In that regard, Figure 7 shows the following trends: (a) $f_{Au\infty}$ increases as the number of slabs in the reactor increases (runs 1 and 3; runs 2 and 4); and (b) $f_{Au\infty}$ increases as $C_{Ab}(0)$ decreases (runs 1 and 4; runs 2 and 3). Based on the previous discussion of eq. (23), such a behavior was expected because in both cases the number of active sites provided for adsorption is increased as one of the operating conditions is changed at a time. As an example, increasing the value of n from 28 to 48 for $C_{Ab}(0) = 5$ mg/L (i.e., runs 1 and 3) causes γ to increase from 1.17 to 2.0 g/mg Au.

On the other hand, it is of interest to note that experiments 1 and 2 in Table III were conducted under different reaction control mechanisms. They also involved the simultaneous changes in both $C_{Ab}(0)$ and n values, which in turn affected the equilibrium values $f_{Au\infty}$. Table III shows that $f_{Au\infty}$ are 0.55 and 0.57 for runs 1 and 2, respectively. At first glance, this may seem contradictory because the membrane-to-gold mass ratio γ was 1.17 and 1.0, respectively. Thus, a higher $f_{Au\infty}$ value for run 1 might be expected. The reason for this apparent discrepancy is the nonlinear nature of eq. (23), in which both $C_{Ab}(0)$ and n were varied simultaneously. In other words, in the expression: $f_{Au\infty} = \gamma q_{A\infty}$, parameter γ is not an independent variable, but it depends on the value of both $C_{Ab}(0)$ and n. For all practical purposes, the small difference in the $f_{Au\infty}$ values for runs 1 and 2 may rely within the experimental uncertainty, and thus it may be assumed that both cases essentially yield equal gold recoveries at equilibrium.

The results presented in Figures 5 through 7 show the potential of the present formulation as a useful tool for the analysis of the adsorption of gold in a CA-PANI membrane in a batch reactor. Provided the adsorption equilibrium relationship [eq. (1)] and the transport properties D_{Aef} and k_m have been determined from appropriate experimental data, similar calculations can be done to improve the kinetics of gold recovery, f_{Au}. By means of eqs. (17) through (23), the model can also be used to estimate the thermodynamic limitations of the reacting system under a variety of experimental conditions, as well as to provide useful information for its further optimization.

CONCLUDING REMARKS

A kinetic model for the adsorption of gold within a porous CA-PANI membrane was developed. The adsorption of gold was represented by an overall ion-exchange reaction in which the AuI_2^- ions replace the Cl^- ions at the active sites of the polyaniline matrix, and the reaction achieves local equilibrium conditions. The rate of adsorption of gold was found to be controlled by the interface mass transfer of the gold complex from the bulk solution to the membrane surface, coupled to the pore diffusion within the membrane matrix. The results of the present formulation indicate that further developments on the synthesis of porous CA-PANI membranes for adsorption applications must focus on increasing the membrane porosity and decreasing its tortuosity. The model shows good potential as a useful tool for the analysis and further optimization of this type of a system.

NOMENCLATURE

a, b, c (mg/L)	Empirical parameters in eq. (3)
Bi (1)	Biot number
C_A (mg/L)	Gold concentration in the aqueous phase within the membrane at time t
$C_{Ab}(t)$ (mg/L)	Gold concentration in the bulk solution at time t
C_{A0}, $C_{Ab}(0)$, C_b^0 (mg/L)	Initial gold concentration in the bulk solution
C_{Aeq} (mg/L)	Equilibrium gold concentration in the aqueous phase
$C_{Aeq}^{cal}(t)$ (mg/L)	Calculated gold concentration in the bulk solution at time t
$C_{Ab}^{exp}(t)$ (mg/L)	Experimental gold concentration in the bulk solution at time t
$C_{As}(t)$ (mg/L)	Gold concentration at the membrane surface at time t

C_i^n, C_i^{n+1} (mg/L)	Gold concentration at node i within the slab at the previous and current time step, respectively.
$\hat{C}_i$ (mg/L)	Average gold concentration in the aqueous phase in the ith finite volume within the membrane
D_{Aef} (cm²/s)	Effective diffusivity of gold within the membrane
D_{Ab} (cm²/s)	Molecular diffusivity of gold in the bulk solution at current concentration
D_{Ab}^0 (cm²/s)	Molecular diffusivity of gold in the bulk solution at infinite dilution
E (mg/L)	Error function of the numerical method
f_{Au}, $f_{Au\infty}$ (1)	Gold recovery at time t and equilibrium, respectively.
k_1 (L/g)	Langmuir isotherm parameter
k_2 (L/mg)	Langmuir isotherm parameter
k_m (cm/s)	Mass transfer coefficient
L (cm)	Length of the square flat slab
m (1)	Number of experimental data
M (1)	Number of nodes in the half-thickness of the flat slab
n (1)	Number of flat slabs in the reactor
p_1 (L/mg)	Parameter defined by eq. (17)
p_2 (1)	Parameter defined by eq. (18)
p_3 (mg/L)	Parameter defined by eq. (19)
q_A (mg/g)	Gold concentration in the solid phase at time t
q_{Aeq} (mg/g)	Equilibrium gold concentration in the solid phase
q_i^n, q_i^{n+1} (mg/g)	Gold concentration at node i within the slab at the previous and current time step, respectively.
$\hat{q}_i$ (mg/g)	Average gold concentration in the solid phase in the ith volume within the membrane
r^2 (1)	Correlation coefficient defined by eq. (14)
S (cm²)	Surface area of an individual slab $= 2L^2$
t (s)	Reaction time
t_1, t_2 (s)	Empirical parameters in eq. (3)
V (L)	Solution volume
w (g)	Weight of membrane in the reactor
z (cm)	Distance from slab centerline

Greek symbols

$\alpha(C_A)$ (cm²/s)	Apparent gold diffusivity defined by eq. (7)
β (1)	Aqueous-to-solid phase volume ratio defined by eq. (21)

γ (1)   Membrane-to-gold mass ratio defined by eq. (24)
δ (cm)   Slab half-thickness
Δt (s)   Numerical time step
Δz (cm)   Numerical size of discretization along the z-axis
ε (1)   Membrane porosity
η_i^n (1)   Numerical parameter in eq. (A2)
λ (1)   Numerical parameter in eqs. (A6) and (A7)
ρ (g/L)   Membrane apparent density
σ (1)   Numerical parameter in eqs. (A6) and (A7)

APPENDIX: NUMERICAL SOLUTION OF THE MATHEMATICAL MODEL

The numerical solution of eq. (6) was performed by means of a semi-implicit finite difference algorithm. The membrane half-thickness δ was discretized into (M-1) small intervals of size Δz with M equally spaced nodes, in which the first node was placed at the centerline of the membrane, and the Mth node was placed at the surface, i.e., $z = \delta$. The process time t was also discretized into N time steps of size Δt. The finite difference approximations of eq. (6) is as follows:

$$\frac{C_i^{n+1} - C_i^n}{\Delta t} = \alpha(C_i^n)\frac{C_{i-1}^n - 2C_i^n + C_{i+1}^n}{(\Delta z)^2}; \quad (A1)$$
$$i = 2...(M-1)$$

where C_i is the concentration of gold in the liquid phase at the ith node within the membrane. In this notation, superscripts n and $n+1$ represent the previous and current time level, respectively, and $\alpha(C_i^n)$ is obtained by replacing C_A by C_i^n into eq. (7). Equation (A1) assumes a forward difference approximation for the time derivative, whereas the spatial derivatives are computed at the previous time step; i.e., it is an explicit formulation. Equation (A1) can be readily solved for the concentration of gold at the current time step to yield:

$$C_i^{n+1} = C_i^n + \eta_i^n(C_{i-1}^n - 2C_i^n + C_{i+1}^n);$$
$$i = 2...(M-1) \quad (A2)$$

where $\eta_i^n = \alpha(C_i^n)(\Delta t)/(\Delta z)^2$. Equation (A2) was used to compute the concentration of gold at the interior

nodes: $i = 2$ through (M-1). The concentration of gold at the center of the membrane C_1^{n+1} was obtained from a Taylor series expansion at $i = 1$ and the substitution of eq. (9) to obtain a finite difference approximation of the second spatial derivative.[35] Further substitution of the resulting expression into eq. (6) yields

$$C_1^{n+1} = C_1^n + 2\eta_1^n(C_2^n - C_1^n) \quad (A3)$$

The concentrations of gold at the membrane surface C_M^{n+1} and that in the bulk solution C_b^{n+1} were computed from the finite difference approximations of eqs. (10) and (11); namely,

$$-D_{\text{Aef}}\frac{C_M^{n+1} - C_{M-1}^{n+1}}{(\Delta z)} = -k_m(C_b^{n+1} - C_M^{n+1}) \quad (A4)$$

and

$$V\frac{(C_b^{n+1} - C_b^n)}{\Delta t} = -Snk_m(C_b^{n+1} - C_M^{n+1}) \quad (A5)$$

Equations (A4) and (A5) are implicit approximations because the spatial derivatives and the interface mass transfer terms are computed at the current time step. The simultaneous solution of eqs. (A4) and (A5) yields

$$C_M^{n+1} = \frac{C_b^n + \lambda(1 + \sigma)C_{M-1}^{n+1}}{1 + \lambda(1 + \sigma)} \quad (A6)$$

and

$$C_b^{n+1} = \frac{C_b^n + \sigma C_M^{n+1}}{1 + \sigma} \quad (A7)$$

where $\lambda = D_{\text{Aef}}/(k_m \cdot \Delta z)$ and $\sigma = Snk_m \cdot \Delta t/V$. An independent estimate of C_b^{n+1} may be computed from eq. (13), which is rewritten as

$$C_b^{n+1} = C_b^0 - \frac{1}{V}\left(2n\varepsilon\sum_{i=1}^{M-1}L^2\hat{C}_i\Delta z + 2n\rho\sum_{i=1}^{M-1}L^2\hat{q}_i\Delta z\right) \quad (A8)$$

where C_b^0 is the initial bulk concentration of gold at time $t = 0$, $\hat{C}_i$, and $\hat{q}_i$ are the average concentrations of gold in the aqueous and solid phases, defined by $\hat{C}_i = 0.5(C_i^{n+1} + C_{i+1}^{n+1})$ and $\hat{q}_i = 0.5(q_i^{n+1} + q_{i+1}^{n+1})$. For the latter expression, the values of q_i^{n+1} were computed from eq. (1) by replacing C_A by C_i^{n+1}. It is noted that the integrals shown in eq. (13) are represented in eq. (A8) by the summation terms, according to the trapezoidal rule of integration.

Equation (A6) shows that the value of C_M^{n+1} depends on the value of C_{M-1}^{n+1}, which is computed from eq. (A2). Likewise, the computation of C_{M-1}^{n+1} from

eq. (A2) depends on the value of C_M^n, which in turn depends on the value of C_{M-1}^n, and so on. This apparently ambiguous formulation arises from the semi-implicit nature of the numerical algorithm. Closure to this problem was provided by the iterative procedure described below.

(1) At the current time step $n+1$, provide a first estimate of the surface concentration at the previous time step, C_M^n.

(2) Compute C_i^{n+1} for nodes: $i = 2$ through (M-1) from eq. (A2), and C_1^{n+1} from eq. (A3). Compute the corresponding q_i^{n+1} values from eq. (1).

(3) Compute C_M^{n+1} from eq. (A6) and C_b^{n+1} from eq. (A7).

(4) Compute an independent estimate of C_b^{n+1} from eq. (A8). For simplicity, this value will be represented by the symbol: G_b^{n+1}.

(5) Compute the error function: $E = C_b^{n+1} - G_b^{n+1}$. If E is sufficiently close to zero, convergence within the current time step has been reached. If not, a new estimate of C_M^n must be provided and steps 2 through 5 must be repeated.

The generation of successive values of C_n^M in step 5 above was done by means of the False-Position method.[35] Convergence criteria were established for both E and the difference between values of C_n^M in two consecutive iterations. A Fortran 90 computer code was written to solve the present model. Upon a series of preliminary calculations to calibrate the code, the numerical parameters were set as follows: $M = 200$ which yields: $\Delta z = 3.19 \times 10^{-4}$cm and $\Delta t = 0.06$s. These values guaranteed the solution to be both stable and not affected by numerical artifacts. Convergence within each time step was typically achieved within one to four iterations.

References

1. Randriamahazaka, H.; Vidal, F.; Dassonville, P.; Chevrot, C.; Teyssie, D. Synth Met 2002, 128, 197.
2. Tallman, D. E.; Wallace, G. G. Synth Met 1997, 90, 13.
3. Wang, P.; Tan, K. L.; Kang, E. T.; Neoh, K. G. Appl Surf Sci 2002, 193, 36.
4. McCarthy, P.; Huang, J.; Yang, S. C.; Wang, H. L. Langmuir 2002, 18, 259.
5. Kinlen, P. J.; Liu, J.; Ding, Y.; Graham, C. R.; Remsen, E. E. Macromolecules 1998, 31, 1735.
6. Madathil, R. Synth Met 2005, 150, 123.
7. Prón, A.; Zagorska, M.; Nicolau, Y.; Genoud, F.; Nechtschein, M. Synth Met 1997, 84, 89.
8. Neves, S. D.; De Paoli, M. A. Synth Met 1998, 96, 49.
9. Al-Ahmed, A.; Mohammad, F.; Rahman, M. Z. Synth Met 2004, 144, 29.
10. Niziol, J.; Laska, J. Synth Met 1999, 101, 720.
11. Wan, M.; Li, M.; Li, J.; Liu, Z. Thin Solid Film 1995, 259, 188.
12. Pereira da Silva, J. E.; Córdoba de Torresi, S. I.; Torresi, R. M. Corros Sci 2005, 47, 811.
13. Rodriguez, F.; Castillo-Ortega, M. M.; Encinas, J. C.; Grijalva, H.; Brown, F.; Sanchez-Corrales, V. M.; Castano, V. M. J Appl Polym Sci 2009, 111, 1216.
14. Kozin, L. F.; Melekhin, V. T. Russ J Appl Chem 2004, 77, 1573.
15. Rodriguez, F.; Castillo-Ortega, M. M.; Encinas, J. C.; Sanchez-Corrales, V. M.; Perez-Tello, M.; Munive, G. T. J Appl Polym Sci 2009, 113, 2670.
16. Hiskey, J. B.; Atluri, V. P. Miner Process Extract Metall Rev 1988, 4, 95.
17. Qi, P. H.; Hiskey, J. B. Hydrometallurgy 1993, 32, 161.
18. Davis, A.; Tran, T.; Young, D. R. Hydrometallurgy 1993, 32, 143.
19. Qiu, H.; Lv, L.; Pan, B. C.; Zhang, Q. J.; Zhang, W. M.; Zhang, Q. X. J Zhejiang Univ Sci A 2009, 10, 716.
20. Banat, F.; Al-Asheh, S.; Makhadmeh, L. Adsorp Sci Technol 2003, 21, 597.
21. Aksu, Z.; Kabasakal, E. Separat Purif Technol 2004, 35, 223.
22. Namasivayam, C.; Sangeetha, D. Chemosphere 2005, 60, 1616.
23. Yan, G. Y.; Viraraghavan, T. Water Res 2003, 37, 4486.
24. Tan, I. A. W.; Ahmad, A. L.; Hameed, B. H. J Hazard Mater 2008, 154, 337.
25. Moreira, R. D. P. M.; Sauer, T. P.; Casaril, L.; Humeres, E. J Appl Electrochem 2005, 35, 821.
26. Evans, J. R.; Davids, W. G.; MacRae, J. D.; Amirbahman, A. Water Res 2002, 36, 3219.
27. Barboza, M.; Almeida, R. M. R. G.; Hokka, C. O. Bioseparation 2001, 10, 221.
28. Barboza, M.; Almeida, R. M. R. G.; Hokka, C. O. Ind Eng Chem Res 2002, 41, 5789.
29. Lu, Y. M.; Wilkins, E. J Hazard Mater 1996, 49, 165.
30. Palacio, L.; Prándanos, P.; Calvo, J. I.; Hernández, A. Thin Solid Film 1999, 348, 22.
31. S. B. Dove. UTHSCSA 2002.
32. Press, W. H.; Teukolsky, S. A.; Vetterling, W. T.; Flannery, B. P. Numerical Recipes in Fortran 77; Cambridge University Press: Cambridge, UK, 1986.
33. Hines, A. L.; Maddox, R. N. Mass Transfer: Fundamentals and Applications; Prentice-Hall: New Jersey, 1984.
34. Cussler, E. L. Diffusion—Mass Transfer in Fluid Systems; Cambridge University Press: Cambridge, UK, 1997.
35. Carnahan, B.; Luther, H. A.; Wilkes, J. O. Applied Numerical Methods; Wiley: New York, 1969.